Further Analysis of the Lens Phenotype in *Lim2*-Deficient Mice

Yanrong Shi,[1] *Alicia B. De Maria,*[1] *Huan Wang,*[2] *Richard T. Mathias,*[2] *Paul G. FitzGerald,*[3] *and Steven Bassnett*[1]

Purpose. Lim2 (MP20) is the second most abundant integral protein of lens fiber cell membranes. A comparative analysis was performed of wild-type and *Lim2*-deficient ($Lim2^{Gt/Gt}$) mouse lenses, to better define the anatomic and physiologic roles of Lim2.

Methods. Scanning electron microscopy (SEM) and confocal microscopy were used to assess the contribution of *Lim2* to lens tissue architecture. Differentiation-dependent changes in cytoskeletal composition were identified by mass spectrometry and immunoblot analysis. The effects on cell–cell communication were quantified using impedance analysis.

Results. *Lim2*-null lenses were grossly normal. At the cellular level, however, subtle structural alterations were evident. Confocal microscopy and SEM analysis revealed that cortical $Lim2^{Gt/Gt}$ fiber cells lacked the undulating morphology that characterized wild-type fiber cells. On SDS-PAGE analysis the composition of cortical fiber cells from wild-type and *Lim2*-null lenses appeared similar. However, marked disparities were evident in samples prepared from the lens core of the two genotypes. Several cytoskeletal proteins that were abundant in wild-type core fiber cells were diminished in the cores of $Lim2^{Gt/Gt}$ lenses. Electrophysiological measurements indicated a small decrease in the membrane potential of $Lim2^{Gt/Gt}$ lenses and a two-fold increase in the effective intracellular resistivity. In the lens core, this may have reflected decreased expression levels of the gap junction protein connexin 46 (Cx46). In contrast, increased resistivity in the outer cell layers of $Lim2^{Gt/Gt}$ lenses could not be attributed to decreased connexin expression and may reflect the absence of cell fusions in $Lim2^{Gt/Gt}$ lenses.

Conclusions. Comparative analysis of wild-type and *Lim2*-deficient lenses has implicated *Lim2* in maintenance of cytoskeletal integrity, cell morphology, and intercellular communication. (*Invest Ophthalmol Vis Sci.* 2011;52:7332–7339) DOI: 10.1167/iovs.11-7724

Lim2 belongs to Pf00822, a family of small (160-173 amino acids), integral membrane glycoproteins that includes epithelial membrane protein 1-3 (EMP 1-3), peripheral myelin protein 22 (PMP-22), and claudins. Members of this family are believed to have a tetraspan topology, with four transmembrane helices and a conserved W-GLW-C-C motif in the first extracellular loop.[1] Mass spectrometric analysis of bovine lenses indicates that, in vivo, Lim2 is phosphorylated near the C terminus, at Ser-170 and, to a lesser degree, at Thr-171. The monophosphorylated form is believed to predominate, although diphosphorylated and unphosphorylated proteins are also present.[2]

Shotgun proteomic studies place Lim2 second only to aquaporin 0 (Aqp0) in apparent abundance in the fiber cell membrane,[3] and a microarray-based expression atlas of multiple tissue and cell types suggests that Lim2 is essentially a lens-specific protein.[4]

Lim2 is conserved across the vertebrate lineage (from mammals to zebrafish[5]), implying that it has important functions in the lens, the only tissue in which it is known to be expressed at significant levels.[4] Genetic analyses in mice and humans indicate that *Lim2* has an indispensible role in lens cell biology.[6] Mutations in *Lim2* underlie cataract formation in the *To3* mouse mutant,[7] perhaps through a dominant negative mechanism.[8] The *Aca47* mouse, identified in a mutagenesis screen, harbors a cysteine-to-arginine substitution at position 51 in *Lim2*, resulting in a small, cataractous lens phenotype.[9] In humans, two recessive mutations in *LIM2* are associated with inherited forms of cataract: a missense mutation (Gly154Glu) is linked to congenital cataract,[10] and a Phe105Val substitution underlies presenile cataract.[11]

The *Lim2* locus has been disrupted in mice using the gene-trap (Gt) technique, effectively resulting in a null allele.[12] Lenses from $Lim2^{Gt/Gt}$ mice were comparable in size and shape to wild-type lenses but, with age, developed faint pulverulent cataracts.[12] Laser analysis of isolated lenses revealed that, although the tissue was largely transparent, the internal refractive properties of *Lim2*-null lenses were disturbed. Despite these and other observations, no clearly defined function for *Lim2* has emerged. It has been suggested that Lim2 may have an adhesive role, although evidence of this is indirect. In rats, Lim2 is incorporated into fiber cell membranes in a region of the lens that becomes impenetrable to extracellular tracers,[13] consistent with the notion that Lim2 promotes close association of adjacent cells.[14] An adhesive role is also suggested by the observation that lenses from *Lim2*-deficient mice are more readily dissociated into constituent cells than are those from wild-type mice.[12]

From the [1]Department of Ophthalmology and Visual Sciences; Washington University School of Medicine; St. Louis, Missouri; the [2]Department of Physiology and Biophysics; SUNY at Stony Brook; Stony Brook, New York; and the [3]Department of Cell Biology and Human Anatomy; School of Medicine; University of California; Davis, California.

Supported by National Eye Institute Grant R01EY018185 (SB), R01EY008747 (PGF), and R01EY006391 (RTM); Core Grants for Vision Research P30EY002687 (WU) and P30 EY12576 (University of California Davis); and an unrestricted grant to the Department of Ophthalmology and Visual Sciences from Research to Prevent Blindness (RPB). Proteomic analysis was performed at the Siteman Cancer Center Proteomics Core Facility, which is supported in part by National Cancer Institute Grant P30 CA91842. SB is the recipient of an RPB Wasserman award.

Submitted for publication April 11, 2011; revised June 29, 2011; accepted July 2, 2011.

Disclosure: **Y. Shi**, None; **A.B. De Maria**, None; **H. Wang**, None; **R.T. Mathias**, None; **P.G. FitzGerald**, None; **S. Bassnett**, None

Corresponding author: Steven Bassnett, Department of Ophthalmology and Visual Sciences, Washington University School of Medicine, 660 South Euclid Avenue, Campus Box 8096, St. Louis, MO 63110; bassnett@vision.wustl.edu.

A recent report provided evidence that *Lim2* may also function in lens intercellular communication.[13] In avian and rodent lenses, proteins and other macromolecules diffuse from cell-to-cell within the body of the lens.[15,16] The conduits for intercellular protein diffusion are believed to be regions of limited cellular fusion.[15] Shi et al.[13] used induced expression of green fluorescent protein (GFP) to visualize intercellular diffusion in mouse lenses directly. Significantly, on a *Lim2*$^{Gt/Gt}$ background, GFP diffusion did not occur and cellular fusions failed to form. Thus, *Lim2* appears to be required for formation or maintenance of the lens syncytium.

The relationship between Lim2-dependent diffusion of large molecules and gap junction–mediated diffusion of ions and other small molecules is unclear. It has long been appreciated that fiber cells are electrically very well coupled.[17] This phenomenon has been ascribed to the presence of numerous gap junctions that conjoin the fiber cell membranes.[18] Lens fiber cells express two gap junction proteins: connexin46 (Cx46) and connexin50 (Cx50). Whereas macromolecules do not permeate gap junctions, ions and small metabolites are expected to diffuse from cell-to-cell through cellular fusions. Were they sufficiently numerous, cellular fusions could therefore contribute significantly to the electrical properties of the lens. A comparative electrophysiological study of wild-type lenses and *Lim2*$^{Gt/Gt}$ lenses (in which membrane fusions do not form) offers an opportunity to parse the contributions of the two, coexisting intercellular pathways.

In the present study, we extended our analysis of the lens of *Lim2*$^{Gt/Gt}$ mice. We show that the absence of *Lim2* is associated with accelerated breakdown of key cytoskeletal proteins in central lens cells. Structural studies revealed concomitant changes in the three-dimensional shape and packing arrangement of lens fiber cells in *Lim2*-null animals. Morphologic changes were accompanied by alterations in the electrophysiological properties of the lens fiber cell membranes and an increase in intracellular resistivity. Together with previous studies, the present data indicate that *Lim2* has indispensible roles in multiple aspects of the fiber cell differentiation process.

Materials and Methods

Animals

The generation of *Lim2*-deficient animals (*Lim2*$^{Gt/Gt}$) has been described previously.[12] *Lim2*$^{Gt/Gt}$ mice were genotyped to exclude the presence of a deletion mutation in the gene for lens beaded filament structural protein-2 (*Bfsp2*) which has previously been detected in 129 and FVB/N mouse strains.[19,20] Wild-type (C57/BL6) mice were obtained from The Jackson Laboratory (Bar Harbor, ME). Mice (aged 1–2 months) were killed by CO_2 asphyxiation. The lenses were dissected from the eye through an incision in the posterior of the globe. All procedures described herein were approved by the Washington University Animal Studies Committee and performed in accordance with the ARVO Statement for the Use of Animals in Ophthalmic and Vision Research.

Single Cell Imaging

Lenses were dissected from age-matched wild-type or *Lim2*$^{Gt/Gt}$ mice and fixed for 5 hours in 4% paraformaldehyde/PBS, as described.[21] Fixed lenses were cut in half along the optic axis to expose the cellular strata. With fine forceps, individual cells and/or bundles of cells were dissected from specific layers of the lens. We divided the lens fiber mass into seven layers of approximately equal thickness, as described.[22] The innermost cell layer was designated layer 0 and the outermost fiber cells were assigned to layer 6. Fiber cells dissected from each layer were dried onto polylysine-coated slides. The cells were then permeabilized with 0.1% Triton X-100 for 5 minutes, blocked with 3% BSA for 30 minutes and incubated overnight in 1:100 dilution of rabbit anti-human AQP0 (AQP01-A; Alpha Diagnostics, San Antonio, TX) and either 1:50 dilution of goat anti-mouse Cx46 (SC-20861; Santa Cruz Biotechnology, Inc., Santa Cruz, CA) or 1:50 dilution of goat anti-human Cx50 (SC-20876; Santa Cruz Biotechnology, Inc.). AQP0 immunofluorescence was used to visualize the surface morphology of the cells. Cells were washed several times in PBS and incubated for 2 hours with 1:200 dilution of Alexa543-conjugated goat anti-rabbit antibody or 1:150 dilution of Alexa488-conjugated chicken anti-goat antibody (Invitrogen, Carlsbad, CA). Cells were washed, mounted in anti-fade reagent (Prolong; Invitrogen), coverslipped, and examined by confocal microscopy. A through-focus set of optical sections was obtained using a confocal microscope (LSM510; Carl Zeiss, Thornwood, NY). Images were collected using an alpha plan fluar 100× (NA 1.45) objective. Electronic zoom was set to 3.0, resulting in x, y pixel dimensions of 40 nm. The z interval was 100 nm. The point-spread function (PSF) of the microscope was distilled from through-focus image stacks of subresolution (170-nm diameter) fluorescent beads (PS-Speck; Invitrogen). The measured PSF was used to deconvolve the stacks of fiber cell images using image-processing software (Huygens Essential, version 3.4; Scientific Volume Imaging [SVI], Hilversum, The Netherlands). The deconvolved image stacks were then rendered (Simulated Fluorescence Process [SFP] Renderer; SVI).

Scanning Electron Microscopy

Lenses were fixed in a mixture of 2% paraformaldehyde and 2.5% glutaraldehyde in 0.1 M sodium cacodylate buffer for 1 hour.[23] Lenses were then split in half along the optic axis and fixed for a further 12 hours. The tissue was dehydrated through acetone, critical point dried, and then split into quarters, yielding fresh fracture surfaces. Specimens were sputter coated and examined with a scanning electron microscope (XL 30; Philips, Andover, MA).

Proteomic Analysis

Lens fiber cell samples from wild-type and *Lim2*$^{Gt/Gt}$ mice were prepared in lysis buffer (Tris-HCl 50 mM [pH 7.4] 1% SDS and protease inhibitor cocktail; Roche Applied Science, Indianapolis, IN). Proteins were separated by electrophoresis on 10% Mes-SDS gels (NuPAGE; Invitrogen), and stained with SYPRO Ruby. Images were acquired with a scanner (Typhoon 9400; GE Healthcare, Piscataway, NJ). Selected gel features were excised robotically and analyzed with a matrix-assisted laser desorption ionization time-of-flight instrument (4700; Applied Biosystems, Inc. [ABI] Foster City, CA). Mass spectrometric analysis was performed by the Proteomics Core at Washington University.

Immunoblot Analysis

Lenses (n = 10–12) were decapsulated and divided into cortical (from the outer 50% of the radius) and core (from the inner 50% of the radius) fractions. The fractions were immediately placed into ice-cold buffer (20 mM Tris-HCl [pH 7.4], 100 mM KCl, 5 mM EDTA, 4 mM DTT, protease inhibitor cocktail; Roche, Indianapolis, IN) and homogenized with 20 strokes of a homogenizer (Dounce; Bellco, Vineland, NJ). Proteins were separated by SDS-PAGE and transferred to nitrocellulose. Blots were incubated with the following primary antibodies: rabbit anti-recombinant mouse filensin (CP115), rabbit anti-mouse CP49 (Bfsp2), chicken anti-recombinant human vimentin (IgY fraction), goat anti-Cx46 (Santa Cruz Biotechnology), goat anti-Cx50 (Santa Cruz Biotechnology), and mouse anti-spectrin (MAB1622; Chemicon, Temecula, CA). Primary antibodies were detected with horseradish peroxidase–conjugated secondary antibodies and enhanced chemiluminescence. A cooled CCD camera (GeneGnome; Syngene, Cambridge, UK) was used for densitometric analysis of the immunoblots. Intensity ratios were computed by dividing the intensity value for the full-length protein in the lens core by the corresponding value in the cortex. Differences between samples were evaluated by two-tailed t-test.

Impedance Analysis

Impedance measurements were performed as described.[24] Briefly, lenses were pinned to the surface of a Sylgard-coated dish by means of four flaps of sclera left attached during the dissection process. Lenses were bathed in Tyrode's solution of the following composition: (mM) 137.7 NaCl, 5.4 KCl, 2.3 NaOH, 2 $CaCl_2$, 1 $MgCl_2$, 10 glucose, 5 HEPES (pH 7.4). The tip of a current-passing microelectrode was inserted into a fiber cell located near the center of the lens and used to inject stochastic current of selected bandwidth. The tip of a second microelectrode was inserted at various depths into the lens. This electrode was used to map out induced voltage in response to the injected current. From these data, the cumulative series resistance (R_s) between the tip of the voltage-recording electrode and the lens surface was measured. Current is believed to flow from the point of injection in the center of the lens to the tissue surface via both intracellular and extracellular routes. If relatively high-frequency (~1 kHz) current is injected, membrane capacitance is short circuited and R_s is proportional to R_p, the parallel resistivity of the effective intracellular resistivity (R_i) and effective extracellular resistivity (R_e). Under normal conditions, R_e is greater than R_i and, therefore, $R_p \approx R_i$. R_i is a measure of the gap junctional coupling resistance. It was assumed in the analyses that R_e does not change significantly between genotypes.

Previous studies in rodent lenses have shown that the composition and distribution of gap junctions varies with radial (and angular) position and that this has implications for the flow of current within the lens.[25] Two functionally distinct compartments have been described. In differentiating fibers (DF; defined as the outer 15% of the lens radius), the cells are relatively well coupled, with a gap junctional conductance [G_j] of 1 S/cm^2 of cell–cell contact.[26] Cells in this outer layer express two kinds of gap junction proteins, Cx46 and Cx50, and both are believed to contribute to cell–cell conductance. At depths greater than 15% of the lens radius (in so-called mature fibers; MF) extensive remodeling of the fiber cell plasma membrane occurs, and many extant proteins are cleaved, including Cx50, the C terminus of which is truncated. In vitro studies suggest that Cx50 truncation reduces macroscopic conductance by almost 90%.[26] Consequently, cell–cell coupling in MF cells is believed to depend almost exclusively on Cx46 and G_j in this region is reduced to approximately half of the value recorded in the DF layer.

Values for R_i in the DF region (R_{DF}) and the MF region (R_{MF}) of wild-type and *Lim2*$^{Gt/Gt}$ lenses were derived from the best fits of equations 1 and 2 to the series resistance measurements:

$$R_S = \frac{R_{DF}}{4\pi}\left(\frac{1}{r} - \frac{1}{a}\right) \quad b \le r \le a \tag{1}$$

$$R_S = \frac{R_{DF}}{4\pi}\left(\frac{1}{b} - \frac{1}{a}\right) + \frac{R_{MF}}{4\pi}\left(\frac{1}{r} - \frac{1}{b}\right) \quad 0 \le r \le b \tag{2}$$

where a is the lens radius (in centimeters); b is location of the DF/MF boundary, and r is the distance of voltage recording electrode from the center of the lens. The specific coupling conductance (conductance per unit area of cell–cell contact) was calculated from $G_{DF} = 1/wR_{DF}$ and $G_{MF} = 1/wR_{MF}$, where R_{DF} and R_{MF} are defined in equations 1 and 2 and w is 3×10^{-4} cm.

Results

Structural Analysis

Although, with time, *Lim2*$^{Gt/Gt}$ lenses exhibit faint pulverulent cataracts, the gross appearance of such lenses is normal.[12] *Lim2*$^{Gt/Gt}$ lenses are also indistinguishable from age-matched, wild-type lenses on conventional histologic examination.[12] To determine whether the absence of *Lim2* may be associated with other, more subtle, morphologic deficits, a combination of confocal microscopy and scanning electron microscopy (SEM) was used.

Individual lens fiber cells were dissected from fixed wild-type and *Lim2*$^{Gt/Gt}$ lenses and visualized by confocal microscopy (Fig. 1). As noted previously,[22] fiber cell morphology varied significantly with depth. In either genotype, the outer cell layers (layers 5 and 6) featured smooth, straight (rectilinear), ribbonlike cells. In layer 4 (located in the midcortex of the lens, approximately 200 μm beneath the surface), wild-type cells had an undulating shape, as described.[21] In contrast, fiber cells dissected from layer 4 of *Lim2*$^{Gt/Gt}$ lenses were rectilinear rather than undulating in shape. Immunofluorescence localization of Cx46 and Cx50 in layer 4 and 5 fiber cells did not reveal

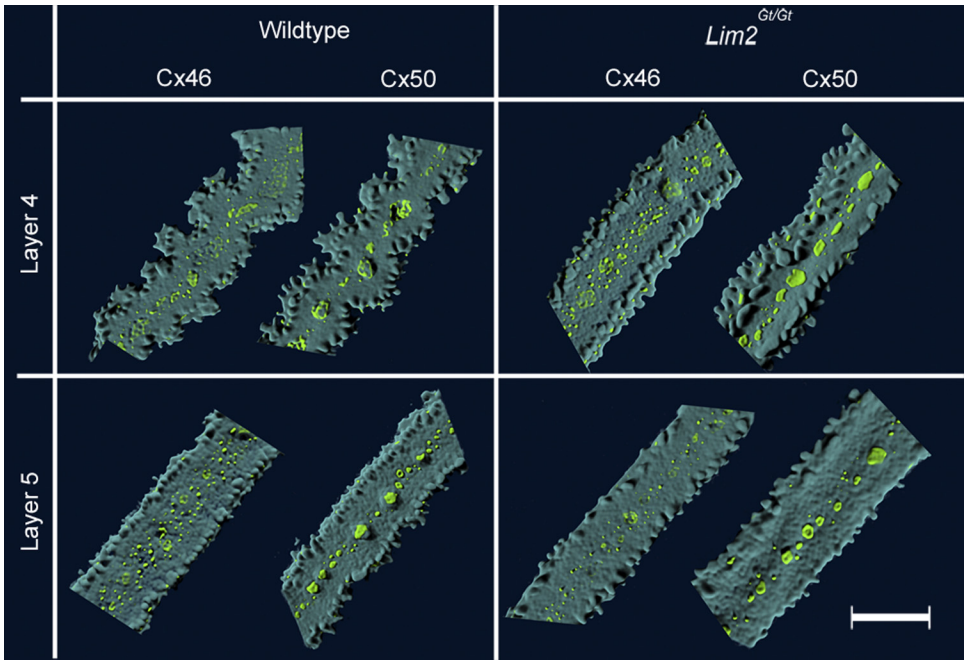

Figure 1. Fiber cell morphology and gap junctional organization in lenses from wild-type and *Lim2*$^{Gt/Gt}$ mice. Individual fiber cells were dissected from layers 4 and 5 of the lens and imaged by confocal microscopy. In layer 5 (~50 μm below the surface), fiber cells from both genotypes were rectilinear in shape and gap junction plaques (*green*) were restricted to the center of the broad faces of the fiber cells. Further into the lens (layer 4; ~200 μm below the surface), wild-type fiber cells had an undulating form, whereas *Lim2*$^{Gt/Gt}$ fibers retained the rectilinear morphology characteristic of the outer (layer 5) cells. Scale bar, 10 μm.

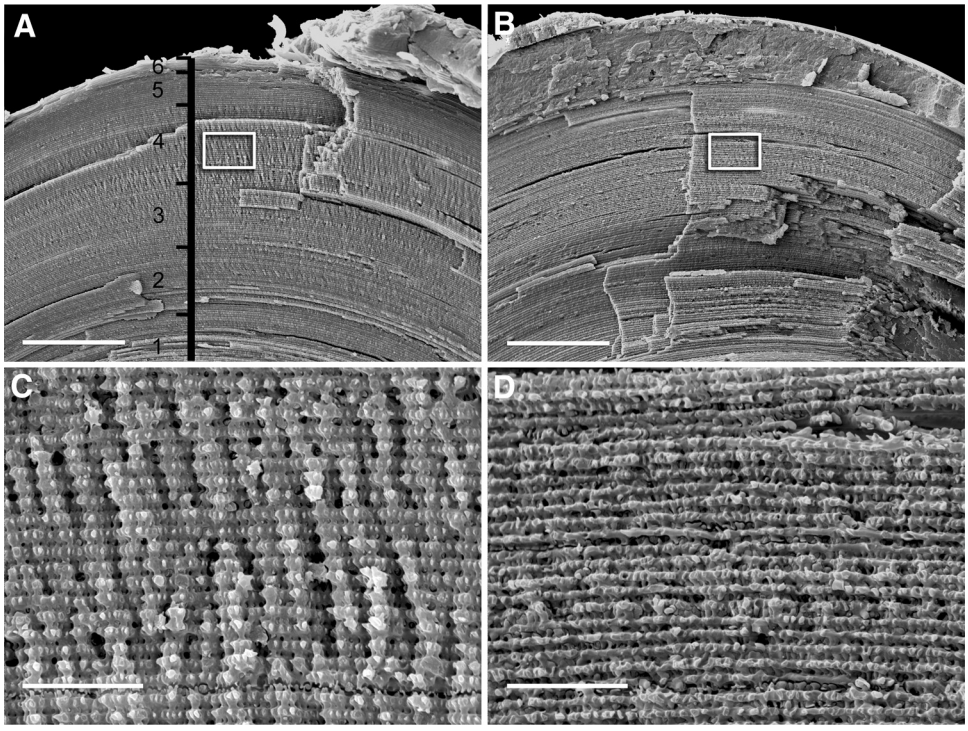

FIGURE 2. Scanning electron micrographs of fiber cells in wild-type (**A**, **C**) and *Lim2*$^{Gt/Gt}$ lenses (**B**, **D**). Lenses were fractured along the optical axis to expose the laminar substructure of the tissue (**A**, **B**). In (**A**), the depth gauge indicates the approximate location of the strata from which cells were dissected for confocal imaging (Fig. 1). Boxed regions in (**A**) and (**B**) are shown at higher magnification in (**C**) and (**D**), respectively. Vertical ridges in the fracture face (**C**) are caused by in-phase undulations in successive layers of fiber cells (see explanatory drawing in Fig. 3). In *Lim2*-deficient lenses (**D**), cortical fiber cells have a rectilinear rather than undulating shape. Consequently, the fractured surface appears smooth rather than ridged. Scale bars: (**A**, **B**) 100 μm; (**C**, **D**) 10 μm.

any significant differences in abundance or distribution of gap junction proteins between the two genotypes. The morphology of cells from layers 0 to 3 was indistinguishable between the two genotypes (data not shown). To corroborate the single cell confocal analysis, fixed lenses were fractured open along the optic axis to expose their laminar substructure and examined by scanning electron microscopy (Fig. 2). In the cortical region (layer 4) of wild-type lenses, the fracture face had a fluted appearance because of the presence of regularly spaced radial ridges (Fig. 2A). Higher magnification images revealed that the radial ridges consisted of undulating fiber cells viewed from their lateral aspect (Fig. 2C). The undulations in one layer of cells were in phase with those of adjacent fiber cell layers (see also the explanatory drawing in Fig. 3). Radial ridges were not present in *Lim2*$^{Gt/Gt}$ lenses (Fig. 2B), as confirmed by higher magnification images (Fig. 2D). Thus, the SEM analysis was consistent with single cell imaging results (Fig. 1).

To examine whether the absence of Lim2 influenced the expression of other membrane or cytoskeletal components, proteins were isolated from the cortical or core regions of wild-type and *Lim2*$^{Gt/Gt}$ lenses and separated by gel electrophoresis. Cursory inspection of the resulting gels revealed that, whereas samples isolated from the lens cortex were indistinguishable, differentially expressed bands were present in the core region (data not shown). Some differentially expressed bands were excised robotically from the gel. Mass spectrometric analysis revealed that, among the differentially expressed proteins were the cytoskeletal components spectrin, vimentin, CP49, and filensin. To verify the differential expression of these proteins, we performed quantitative immunoblot analysis. Representative gels are shown in Figure 4A and corresponding densitometric data are shown in Figure 4B and 4C.

In all cases, proteins were present as multiple bands on immunoblots (Fig. 4A), presumably reflecting the many post-translational modifications that cytoskeletal elements undergo during fiber cell terminal differentiation.[27,28] In the cortical samples, the pattern of proteolytic fragments was indistinguishable between wild-type and *Lim2*$^{Gt/Gt}$ lenses. Consequently, the protein expression ratios (computed from the relative abundance of the full-sized protein) were close to unity for the two genotypes (Fig. 4B). In wild-type lenses, there was a significant decrease in the abundance of full-length protein in the core samples compared with the cortical samples (Fig. 4C). The intensity ratios (core intensity/cortical intensity) ranged from approximately 0.1 for spectrin to 0.9 for CP49 and most likely reflect proteolysis occurring during the latter stages of fiber differentiation. In *Lim2*$^{Gt/Gt}$ lenses, this process was even more marked. As a result, proteins such as vimentin were barely detectable in the core of *Lim2*$^{Gt/Gt}$ lenses (Fig. 4A). For each of the proteins, there was a statistically significant decrease in intensity ratio compared to wild-type (Fig. 4C). To-

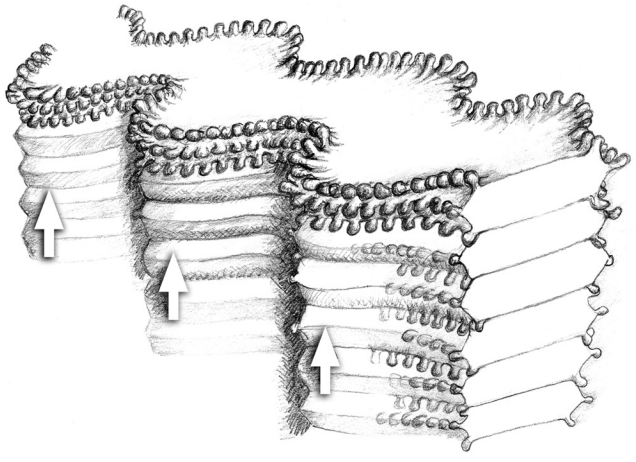

FIGURE 3. Fiber cell packing arrangement in the cortical region (layer 4) of wild-type lenses. The fiber cells are highly elongated, with a flattened, hexagonal cross section. Fingerlike protrusions extend from the six cell vertices. The undulating morphology of one fiber cell is in phase with undulations in the cells above and below. When viewed from the lateral aspect, therefore, a column of fiber cells has a fluted appearance, with in-phase undulations forming a series of radially oriented ridges (*arrows*) in the tissue face (compare with Fig. 2C).

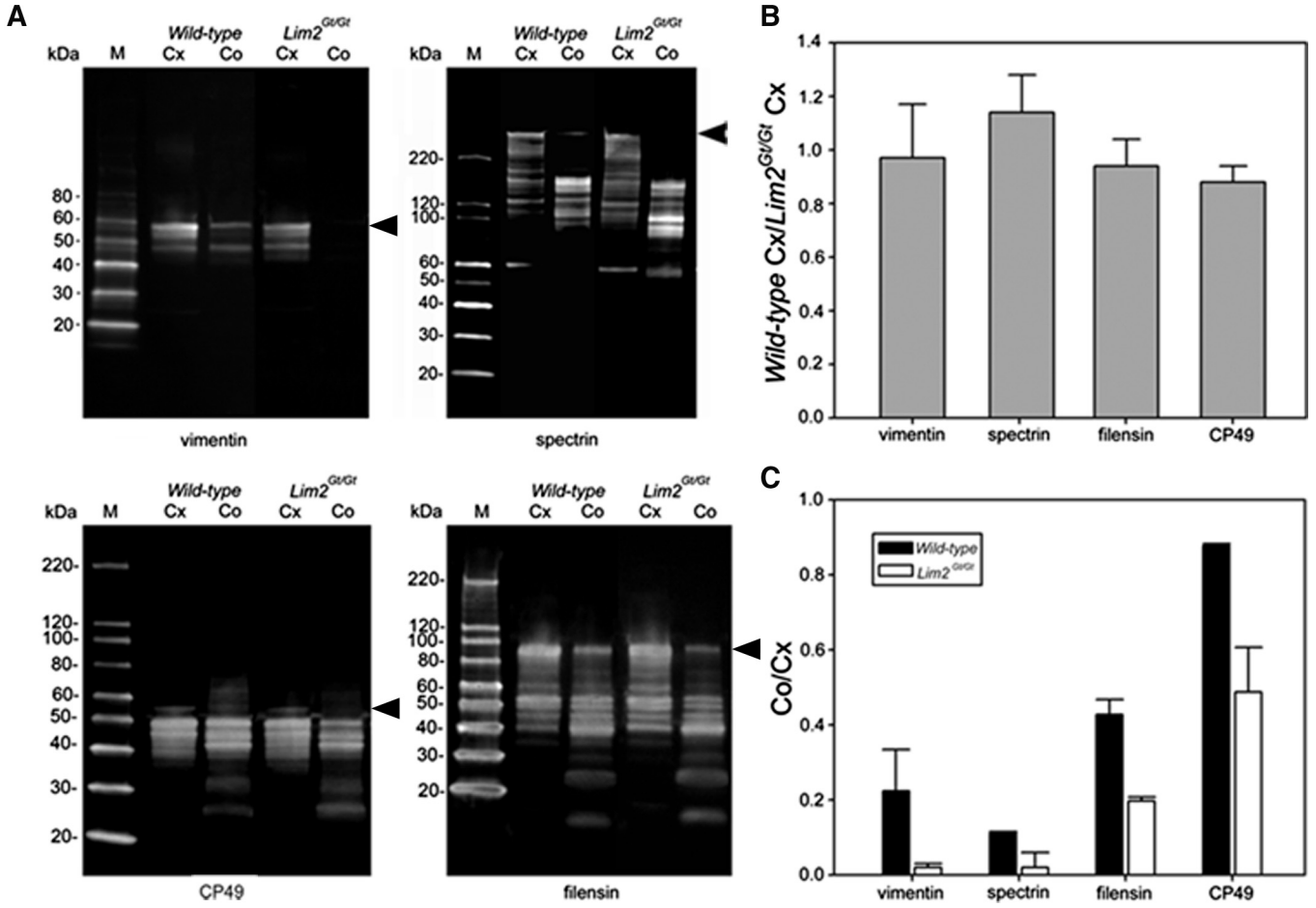

Figure 4. Differential expression patterns of cytoskeletal proteins in the cortex (Cx) and core (Co) of wild-type and *Lim2*$^{Gt/Gt}$ lenses. (**A**) Immunoblot analysis of vimentin, spectrin, CP49, and filensin expression. In wild-type lenses, the full-length forms of each protein (*arrowheads*) were reduced in abundance in the core samples relative to the cortical samples. Although the expression level of each protein was similar (expression ratio close to 1) in cortical samples from wild-type and *Lim2*$^{Gt/Gt}$ lenses (**B**), the expression level in the core of the *Lim2*$^{Gt/Gt}$ lenses was significantly ($P < 0.05$) reduced compared with core the samples from wild-type lenses (**C**). The data in (**B**) and (**C**) represent the averages ± SD of three independent determinations.

gether, these data suggest that the degradation of the cytoskeleton observed during the course of normal fiber cell maturation is accelerated significantly in *Lim2*$^{Gt/Gt}$ lenses.

Impedance Analysis

Lim2 expression is necessary for the formation of membrane fusions in the lens and the subsequent intercellular diffusion of proteins.[13] Fusions are also expected to facilitate the intercellular flow of ions and small molecules, but their contribution to the electrical properties of the lens has not been defined. To gain insights into the physiological role of *Lim2*, we performed a comparative electrical impedance study of wild-type and *Lim2*$^{Gt/Gt}$ lenses.

Lens input resistance, measured near the surface of the tissue, was indistinguishable between wild-type and *Lim2*$^{Gt/Gt}$ lenses (Table 1), suggesting that the absence of Lim2, a major component of the fiber cell membrane, did not have untoward effects on membrane integrity. However, membrane potential was slightly, but significantly depolarized, indicating that the permeability properties of the mutant lenses were somewhat altered. Figure 5 shows R_s data from wild-type and *Lim2*$^{Gt/Gt}$ lenses and the curve fit of equations 1 and 2 to the data. Compared to wild-type, R_s was greater at all radial locations in *Lim2*$^{Gt/Gt}$ lenses. It is qualitatively evident, therefore, that cell–cell coupling was reduced throughout *Lim2*$^{Gt/Gt}$ lenses. The averaged best-fit values for wild-type lenses were R_{DF} = 6.0 kΩ · cm and R_{MF} 9.2 kΩ · cm and for *Lim2*$^{Gt/Gt}$ were R_{DF} 13.2 kΩ · cm and R_{MF} = 20.1 kΩ · cm. Coupling conductance per unit area of cell-to-cell contact for each genotype is shown in Table 2. On average, the absence of Lim2 was associated

Table 1. Electrophysiological Properties of Wild-Type and *Lim2*$^{Gt/Gt}$ Lenses

	Wild-Type (n = 19 Lenses from 11 Mice)	*Lim2*$^{Gt/Gt}$ (n = 13 Lenses from 7 Mice)	P
Input resistance, kΩ	3.6 ± 0.5	3.4 ± 0.6	0.61
Membrane potential, mV	−63 ± 4	−55 ± 5	0.0001

Data represent mean ± SD of n determinations.

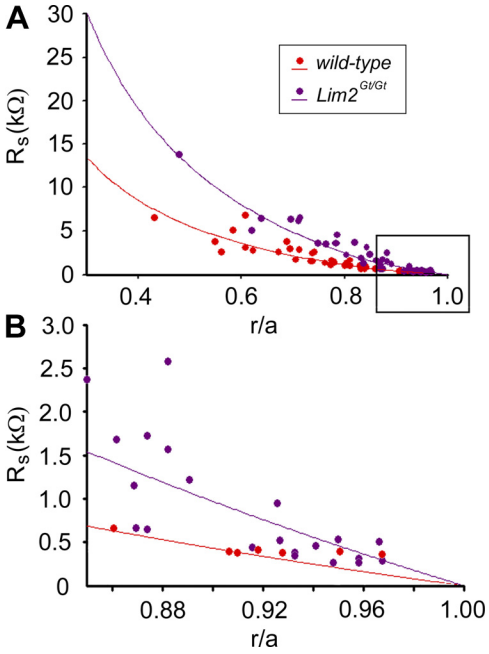

FIGURE 5. R_s between the tip of the voltage-recording electrode located *r* centimeters from the lens center and the surface of a lens of radius *a* centimeters. Data are plotted as a function of the fractional distance (*r*/*a*) from the center of the lens. (**B**) An expanded view of the boxed region from (**A**). This region corresponds to the zone of DF cells.

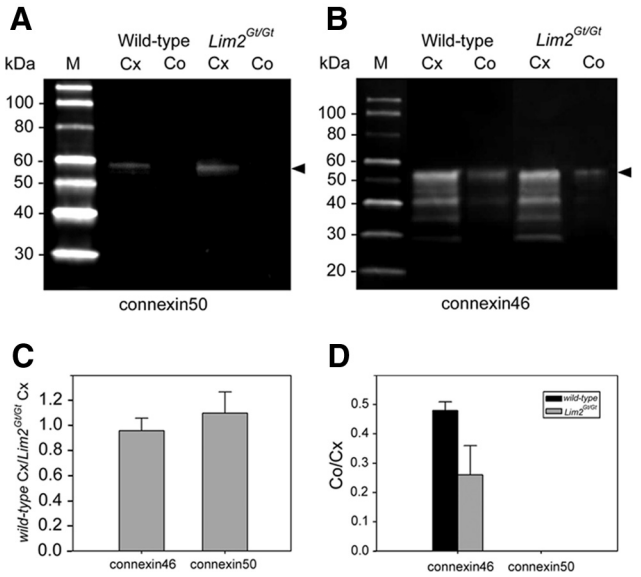

FIGURE 6. Expression levels of Cx46 and Cx50 in the cortex (Cx) and core (Co) of wild-type and *Lim2*$^{Gt/Gt}$ lenses. (**A**) The epitope recognized by the Cx50 antibody was only present in the cortical fraction from the two genotypes. (**B**) Cx46 was detected in the core and cortical fractions of wild-type and *Lim2*$^{Gt/Gt}$ lenses. (**C**) The expression level of Cx46 and Cx50 in the cortices of wild-type and *Lim2*$^{Gt/Gt}$ lenses were indistinguishable. (**D**) The level of Cx46 in the core of *Lim2*$^{Gt/Gt}$ lenses was approximately half that observed in the core of wild-type lenses. The quantitative data shown in (**C**) and (**D**) represent mean ± SD of three independent determinations. *Arrowheads*: full-length protein.

with a 55% decrease in coupling conductance in both the DF and MF regions of the lens.

The twofold increase in cell–cell resistance in the *Lim2*$^{Gt/Gt}$ lens was consistent with the notion that lens fusions account for 50% of the intercellular flow of ions. However, an alternative explanation could be that the absence of Lim2 had directly or indirectly effected connexin expression. To test this possibility, we examined the expression of Cx46 and Cx50 in the core and cortical regions of wild-type and *Lim2*$^{Gt/Gt}$ lenses (Fig. 6). Cx50 was detected at approximately equal levels in cortical samples from wild-type and *Lim2*$^{Gt/Gt}$ lenses but was not detected in core samples from either genotype. The absence of Cx50 signal from the lens core probably reflects truncation of the Cx50 carboxyl terminus during fiber differentiation and loss of the epitope recognized by the Cx50 antibody. The levels of Cx46 were indistinguishable in cortical samples from the two genotypes. However, there was a significant (~50%) reduction in Cx46 abundance in the core samples from *Lim2*$^{Gt/Gt}$ lenses. These data suggest that the increased intercellular resistance in the center of *Lim2*$^{Gt/Gt}$ lenses could be attributed to decreased expression of Cx46 in the absence of Lim2. However, the same argument cannot be made in the outer fiber cell layer, because in that region connexin levels were indistinguishable between the two genotypes as indicated by the immunoblot data (Fig. 6A) and the immunocytochemical results (Fig. 1).

TABLE 2. Coupling Conductance per Unit Area of Cell-to-Cell Contact Calculated from the R_{DF} and R_{MF} Values for Each Genotype

	Wild-Type	*Lim2*$^{Gt/Gt}$
Coupling conductance, S/cm^2 of cell-to-cell contact		
DF	0.56	0.25
MF	0.36	0.16
Normalized coupling conductance		
DF	1.00	0.45
MF	1.00	0.44

DISCUSSION

In recent years, genes encoding several of the most abundant lens membrane proteins (*Aqp0*, *Cdh2*, *Cx46*, and *Cx50*) have been inactivated in mice. Without exception, the knockout phenotypes have been severe.[29–32] The relatively mild lens phenotype observed in *Lim2*$^{Gt/Gt}$ mice thus sets Lim2 apart from the other superabundant lens membrane proteins. Previous studies have shown that *Lim2*$^{Gt/Gt}$ lenses are grossly normal, albeit slightly smaller than age-matched wild-type lenses.[12] Faint, pulverulent opacities develop with age but, at all stages, the lens remains largely transparent. Even on histologic inspection, it is difficult to differentiate between wild-type and *Lim2*$^{Gt/Gt}$ lenses. Some differences between the genotypes have been noted, however. For example, the internal refractive properties of *Lim*$^{Gt/Gt}$ lenses are disturbed.[12] It has also been shown that the intercellular diffusion of proteins, a feature of mature fiber cells in wild-type lenses, does not occur in *Lim2*$^{Gt/Gt}$ lenses.[13] Whether the absence of the intercellular protein diffusion pathway contributes to the development of the refractive anomalies remains to be determined.

In the current manuscript, we extended our morphologic and biochemical analysis of the *Lim2*$^{Gt/Gt}$ lens phenotype. To examine cellular phenotypes in three dimensions and at high spatial resolution, we used a novel technique in which individual fiber cells were dissected from various strata of wild-type or *Lim2*$^{Gt/Gt}$ lenses and visualized by confocal microscopy. Viewed in three dimensions, it was apparent that *Lim2*$^{Gt/Gt}$ and wild-type fiber cells were structurally similar. In each case, the cells had a flattened hexagonal cross section and their

surface membranes were decorated with regularly arranged fingerlike processes that protruded from the cellular vertices and, in life, serve to interconnect the fiber cells. The sole difference in cellular morphology noted in this study was that all *Lim*$^{Gt/Gt}$ fiber cells were rectilinear in shape, whereas fibers isolated from the midcortical strata (layer 4, in the terminology used in this study) of the wild-type lens had an undulating shape. This finding was substantiated by scanning electron microscopy. The significance of this observation is unknown, however. The adoption of the undulating form occurs relatively late in fiber differentiation, in cells undergoing, or about to undergo organelle breakdown.[23] Whether or not the change in cell shape has a specific function in the lens or is merely an epiphenomenon associated with other aspects of the differentiation program is not known. To the best of our knowledge, undulating fiber cells have been reported only in rodent lenses[23]; it is unclear whether these structures are a common feature of vertebrate lenses. Interestingly, a recent report has shown that, in contrast to the situation in *Lim2*$^{Gt/Gt}$ fiber cells (where the mutant fibers are abnormally straight), the absence of the cell–cell adhesion protein *Cadm1* from the lens results in fiber cell undulations of exaggerated amplitude.[21]

The cytoskeleton is remodeled significantly during the terminal differentiation of lens fiber cells. Some components, such as microtubules, that are prominent in the outer cell layers are lost completely during the early stages of differentiation.[33] Other cytoskeletal elements, for example, spectrin, are subjected to progressive proteolysis.[28,34] As a result, immunoblots of cytoskeletal proteins isolated from the entire lens (and thus containing cells at all stages of differentiation) generally reveal families of proteolytic fragments derived from full-sized parent molecules. Quantitative comparisons of key cytoskeletal proteins in lenses from wild-type and *Lim2*$^{Gt/Gt}$ lenses revealed that proteolytic degradation was accelerated significantly in fiber cells isolated from the center of the *Lim2*$^{Gt/Gt}$ lens. The identity of the proteases responsible for cleaving the cytoskeletal substrates is not known but the concomitant degradation of structurally unrelated proteins suggests the involvement of a relatively nonspecific pathway. Calcium-activated proteases, calpains, have been implicated in normal aspects of fiber cell differentiation and in pathologic conditions that culminate in abnormally high concentrations of intracellular calcium in the lens.[28,35] For example, opacification of the nuclear region of lenses deficient in Cx46 is secondary to calcium influx and activation of calpain 3 in central fiber cells.[29,36] The cytoskeletal proteins degraded in the center of *Lim2*$^{Gt/Gt}$ lenses are all well-characterized calpain substrates. We hypothesize, therefore, that the absence of Lim2 results in either increased influx and/or decreased efflux of calcium, as a result of which intracellular calcium accumulates, calpains are activated, and proteolytic cleavage is accelerated. A similar mechanism has been proposed to account for the dense cataracts that develop in the center of Cx46-knockout lenses.[36,37] Further studies are needed to determine whether calcium accumulates in the center of *Lim2*$^{Gt/Gt}$ lenses and the role specific calpains may play.

The availability of *Lim2*$^{Gt/Gt}$ lenses offers an opportunity to parse the contributions of the two intercellular diffusion pathways that coexist in lenses. The cell–cell movement of ions and other small molecules is facilitated by gap junction channels (composed of Cx46 and Cx50). Proteins, however, appear to diffuse from cell-to-cell via regions of cellular fusion.[38] In principle, both pathways could contribute to coupling conductance, but equivalent circuit models have generally neglected the contribution of fusions on the grounds that they were not numerous enough to influence the electrical properties.[39] However, recent GFP tracer studies suggest that intercellular protein diffusion is a property of all but the most superficial fiber cells.[13,15,16,40,41] Furthermore, the uniform distribution of GFP in labeled lenses suggests that most central fiber cells are fused to some degree. It has been shown that fusions do not form in *Lim2*$^{Gt/Gt}$ lenses.[13] Such lenses therefore provide a model in which the contribution of gap junction–mediated conductance can be assessed in the absence of the parallel fusion pathway. Impedance analysis indicated that the intercellular resistance was approximately doubled in *Lim2*$^{Gt/Gt}$ lenses compared to wild-type, consistent with the notion that, in wild-type lenses, 50% of intercellular current flows through cellular fusions. This interpretation was confounded however by the observation that expression levels of Cx46 in the center of *Lim2*$^{Gt/Gt}$ lenses were also significantly reduced. Under these circumstances, the increased resistance in the center of the *Lim2*$^{Gt/Gt}$ lens may equally be attributed to reduced Cx46 expression. An increase in intercellular resistance was also measured in the outer cortical layers. In this region, connexin expression levels in wild-type and *Lim2*$^{Gt/Gt}$ lenses were comparable. It is possible, therefore, that fusions contribute to intercellular current flow in this region. A caveat with comparative analyses such as these is that the deletion of a major component of the membrane proteome inevitably has pleiotropic consequences. We showed that disruption of the *Lim2* locus affects the expression of Cx46. Others have shown the converse, that deletion of fiber cell connexins blocks the intercellular diffusion of proteins, presumably by preventing fusion formation.[40] Further experiments, perhaps employing acute models, will therefore be necessary to definitively parse the contributions of these parallel systems for intercellular diffusion of solutes in the lens.

Acknowledgments

The authors thank Paul FitzGerald (University of California Davis) for providing antibodies to filensin, CP49, and vimentin, and Alan Shiels (Washington University School of Medicine, St. Louis) for kindly providing *Lim2*$^{Gt/Gt}$ mice.

References

1. Van Itallie CM, Anderson JM. Claudins and epithelial paracellular transport. *Annu Rev Physiol.* 2006;68:403–429.
2. Ervin LA, Ball LE, Crouch RK, Schey KL. Phosphorylation and glycosylation of bovine lens MP20. *Invest Ophthalmol Vis Sci.* 2005;46:627–635.
3. Bassnett S, Wilmarth PA, David LL. The membrane proteome of the mouse lens fiber cell. *Mol Vis.* 2009;15:2448–2463.
4. Lattin JE, Schroder K, Su AI, et al. Expression analysis of G protein-coupled receptors in mouse macrophages. *Immunome Res.* 2008;4:5.
5. Vihtelic TS, Fadool JM, Gao J, Thornton KA, Hyde DR, Wistow G. Expressed sequence tag analysis of zebrafish eye tissues for NEIBank. *Mol Vis.* 2005;11:1083–1100.
6. Shiels A, Bennett TM, Hejtmancik JF. Cat-Map: putting cataract on the map. *Mol Vis.* 2010;16:2007–2015.
7. Steele EC Jr, Kerscher S, Lyon MF, et al. Identification of a mutation in the MP19 gene, Lim2, in the cataractous mouse mutant To3. *Mol Vis.* 1997;3:5.
8. Steele EC Jr, Wang JH, Lo WK, Saperstein DA, Li X, Church RL. Lim2(To3) transgenic mice establish a causative relationship between the mutation identified in the lim2 gene and cataractogenesis in the To3 mouse mutant. *Mol Vis.* 2000;6:85–94.
9. Puk O, Ahmad N, Wagner S, Hrabe de Angelis M, Graw J. Microphakia and congenital cataract formation in a novel Lim2 mutant mouse. *Mol Vis.* 2011;17:1164–1171.
10. Ponnam SP, Ramesha K, Tejwani S, Matalia J, Kannabiran C. A missense mutation in LIM2 causes autosomal recessive congenital cataract. *Mol Vis.* 2008;14:1204–1208.
11. Pras E, Levy-Nissenbaum E, Bakhan T, et al. A missense mutation in the LIM2 gene is associated with autosomal recessive presenile

cataract in an inbred Iraqi Jewish family. *Am J Hum Genet.* 2002; 70:1363–1367.
12. Shiels A, King JM, Mackay DS, Bassnett S. Refractive defects and cataracts in mice lacking lens intrinsic membrane protein-2. *Invest Ophthalmol Vis Sci.* 2007;48:500–508.
13. Shi Y, Barton K, De Maria A, Petrash JM, Shiels A, Bassnett S. The stratified syncytium of the vertebrate lens. *J Cell Sci.* 2009;122: 1607–1615.
14. Grey AC, Jacobs MD, Gonen T, Kistler J, Donaldson PJ. Insertion of MP20 into lens fibre cell plasma membranes correlates with the formation of an extracellular diffusion barrier. *Exp Eye Res.* 2003; 77:567–574.
15. Shestopalov VI, Bassnett S. Expression of autofluorescent proteins reveals a novel protein permeable pathway between cells in the lens core. *J Cell Sci.* 2000;113:1913–1921.
16. Shestopalov VI, Bassnett S. Development of a macromolecular diffusion pathway in the lens. *J Cell Sci.* 2003;116:4191–4199.
17. Duncan G. The site of the ion restricting membranes in the toad lens. *Exp Eye Res.* 1969;8:406–412.
18. Mathias RT, White TW, Gong X. Lens gap junctions in growth, differentiation, and homeostasis. *Physiol Rev.* 2010;90:179–206.
19. Simirskii VN, Lee RS, Wawrousek EF, Duncan MK. Inbred FVB/N mice are mutant at the cp49/Bfsp2 locus and lack beaded filament proteins in the lens. *Invest Ophthalmol Vis Sci.* 2006;47:4931–4934.
20. Sandilands A, Wang X, Hutcheson AM, et al. Bfsp2 mutation found in mouse 129 strains causes the loss of CP49′ and induces vimentin-dependent changes in the lens fibre cell cytoskeleton. *Exp Eye Res.* 2004;78:875–889.
21. De Maria A, Shi Y, Luo X, Van Der Weyden L, Bassnett S. Cadm1 expression and function in the mouse lens. *Invest Ophthalmol Vis Sci.* 2011;52:2293–2299.
22. Bassnett S, Shi Y, Vrensen GFJM. Biological glass: structural determinants of eye lens transparency (review). *Phil Trans R Soc Lond B Biol Sci.* 2011;366:1250–1264.
23. Blankenship T, Bradshaw L, Shibata B, Fitzgerald P. Structural specializations emerging late in mouse lens fiber cell differentiation. *Invest Ophthalmol Vis Sci.* 2007;48:3269–3276.
24. Baldo GJ, Gong X, Martinez-Wittinghan FJ, Kumar NM, Gilula NB, Mathias RT. Gap junctional coupling in lenses from alpha(8) connexin knockout mice. *J Gen Physiol.* 2001;118:447–456.
25. Baldo GJ, Mathias RT. Spatial variations in membrane properties in the intact rat lens. *Biophys J.* 1992;63:518–529.
26. Martinez-Wittinghan FJ, Sellitto C, White TW, Mathias RT, Paul D, Goodenough DA. Lens gap junctional coupling is modulated by connexin identity and the locus of gene expression. *Invest Ophthalmol Vis Sci.* 2004;45:3629–3637.
27. Su SP, McArthur JD, Truscott RJ, Aquilina JA. Truncation, cross-linking and interaction of crystallins and intermediate filament proteins in the aging human lens. *Biochim Biophys Acta.* 2011; 1814;647–656.
28. De Maria A, Shi Y, Kumar NM, Bassnett S. Calpain expression and activity during lens fiber cell differentiation. *J Biol Chem.* 2009; 284:13542–13550.
29. Gong X, Li E, Klier G, et al. Disruption of alpha3 connexin gene leads to proteolysis and cataractogenesis in mice. *Cell.* 1997;91: 833–843.
30. White TW, Goodenough DA, Paul DL. Targeted ablation of connexin50 in mice results in microphthalmia and zonular pulverulent cataracts. *J Cell Biol.* 1998;143:815–825.
31. Shiels A, Bassnett S, Varadaraj K, et al. Optical dysfunction of the crystalline lens in aquaporin-0-deficient mice. *Physiol Genomics.* 2001;7:179–186.
32. Pontoriero GF, Smith AN, Miller LA, Radice GL, West-Mays JA, Lang RA. Co-operative roles for E-cadherin and N-cadherin during lens vesicle separation and lens epithelial cell survival. *Dev Biol.* 2009; 326:403–417.
33. Kuwabara T. Microtubules in the lens. *Arch Ophthalmol.* 1968;79: 189–195.
34. Lee A, Morrow JS, Fowler VM. Caspase remodeling of the spectrin membrane skeleton during lens development and aging. *J Biol Chem.* 2001;276:20735–20742.
35. Azuma M, Fukiage C, David LL, Shearer TR. Activation of calpain in lens: a review and proposed mechanism. *Exp Eye Res.* 1997;64: 529–538.
36. Tang Y, Liu X, Zoltoski RK, et al. Age-related cataracts in alpha3Cx46-knockout mice are dependent on a calpain 3 isoform. *Invest Ophthalmol Vis Sci.* 2007;48:2685–2694.
37. Gao J, Sun X, Martinez-Wittinghan FJ, Gong X, White TW, Mathias RT. Connections between connexins, calcium, and cataracts in the lens. *J Gen Physiol.* 2004;124:289–300.
38. Kuszak JR, Macsai MS, Bloom KJ, Rae JL, Weinstein RS. Cell-to-cell fusion of lens fiber cells in situ: correlative light, scanning electron microscopic, and freeze-fracture studies. *J Ultrastruct Res.* 1985; 93:144–160.
39. Mathias RT, Rae JL. Cell to cell communication in the lens. In: Sperelakis N, Cole W, eds. *Cell Interactions and Gap Junctions*. Boca Raton, FL: CRC; 1989:29–50.
40. Cheng C, Xia CH, Li L, White TW, Niimi J, Gong X. Gap junction communication influences intercellular protein distribution in the lens. *Exp Eye Res.* 2008;86:966–974.
41. Shi Y, Bassnett S. Inducible gene expression in the lens using tamoxifen and a GFP reporter. *Exp Eye Res.* 2007;85:732–737.